# Theoretical and Computational Study of Electronic Structure of High Pressure Phases of Bismuth

Monday 10th October, 2016

Supervisor: Dr F. M. Grosche

**Abstract**

In this project, with computation based on Density Functional Theory, several experimentally observed trends were successfully explained. By analysing the evolution of the Fermi surfaces with pressure, it was possible to extract the pressure dependence of the carrier concentration. Computation suggested that the carrier density of Bi-I decreases with pressure until a band gap opens up at $(4.6 \pm 0.4)$ GPa. This successfully explains an experimental trend that its electrical resistivity increases with pressure until it becomes a semiconductor. As pressure was increased further, Bi-I is changed to another phase, Bi-III, (after a brief phase II) with the boundary pressure experimentally found to be approximately 2.5 GPa. Bi-III adopts an incommensurate host-guest structure without a unit cell, which renders precise modelling on a computer impossible. Therefore, progressively accurate models were used to study the properties of Bi-III by analysing the band structures of the approximate models. By comparison of energy densities, Bi-III was shown to be favoured over Bi-I at pressures above $(8.4 \pm 0.4)$ GPa. This crossing of energy-pressure curves demonstrates that the structural change can be understood by numerical modelling, although the pressure at which the crossing occurs does not agree with the experimental data. Calculations also showed that the density of states is non-zero at the Fermi energy of the material, therefore supporting the experimental fact that Bi-III is a metal. In addition, the Bi-III plasma frequency was estimated to be $(3.8 \pm 0.1)$ eV along a direction perpendicular to the symmetry axis, and $(4.5 \pm 0.5)$ eV along the direction parallel the symmetry axis. Barium in its phase IV was also investigated since it has a similar structure to Bi-III. The band structures for the best approximate models of Bi-III and Ba-IV were obtained, and can be used to improve our understanding of the incommensurate host-guest structures in general. In this project, I have used different degrees of approximations and looked for a compromise between decreasing computing time and improving accuracy. Some of the results of the project will provide a theoretical basis for the corresponding experimental observations and measurements at the Shoenberg Laboratory for Quantum Matter, University of Cambridge.

# Contents

# 1 Introduction

The Quantum Matter (QM) Group at Cavendish Laboratory investigates properties of materials under extraordinary conditions such as high pressures, high magnetic fields and extremely low temperatures [1]. The group has obtained a range of data on the properties of bismuth preceding this project. Some brief results are as follows [2]. Elemental bismuth displays an unusually low carrier concentration of the order of 1 carrier in 100,000 atoms, and this is reduced further under applied pressure. Experiments suggested that a band gap opens up at the Fermi level at a pressure of merely about $(1.4 \pm 0.6)$ GPa. Moreover, bismuth changes into an incommensurate host-guest structure above 2.5 GPa, in which it displays metallic behaviour and becomes superconducting below about 7.1 K. Figure 1 shows a phase diagram which illustrates key aspects of the pressure-dependent properties of bismuth.

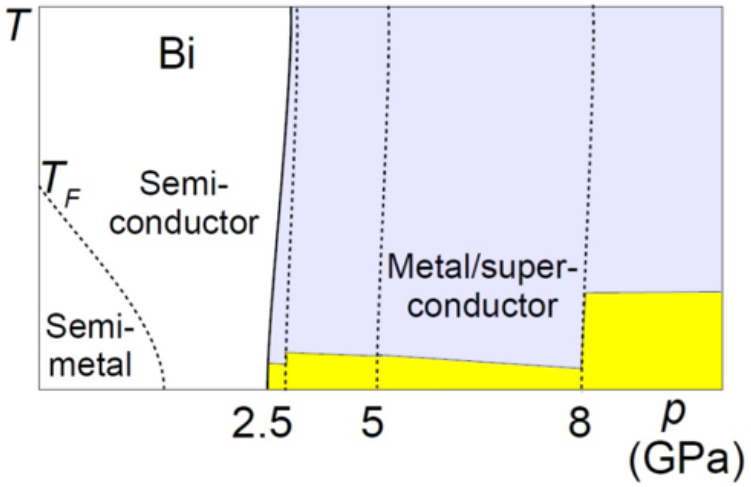


*Figure 1: A phase diagram for bismuth [2, 3]. The uncoloured section is Bi-I, and the coloured section is Bi-III. The yellow section is the superconductor phase.*

From meters down to micrometers, classical theories can be used to investigate the properties of materials. However, on a nanometer scale, it is the quantum electronic structure that determines the properties of the solid. In this project, I investigated the evolution of the electronic structure of bismuth with pressure using numerical calculations based on Density Functional Theory (DFT). I explored both the low pressure behaviour, successfully reproducing the semimetal to semiconductor transition, and the high pressure behaviour pertaining to Bi-III. For the latter, I created a series of commensurate structures approximating the incommensurate Bi-III structure, in which the band structure calculations are feasible. In addition, I investigated similarities between Bi-III and Ba-IV which have the same type of structure but with different parameters.

In physics, when theories and models exist, experimental data are obtained to test them. In other cases, however, when no theories exist, experimental data are obtained so that

theories can be proposed according to them. In either situation, some measurable quantities must come out of the theory. In condensed matter physics, there are a range of theories making different assumptions, with the simple ones usually being valid only for very limited conditions. As a result, when the simple theories do not work, it is more difficult to obtain valid measurable theoretical predictions. In this project, I carried out most of the calculations not by using simplified models but by using Density Functional Theory. Due to the intrinsically large number of computational steps and large amount of memory required, most of the calculations were carried out on a computer.

The computations were predominantly carried out with the computer program `WIEN2k`, but other computer programs such as `VESTA`, `XCrysDen` and `SKEAF` were also used for writing input files, visualising the Fermi surfaces, processing the output files, etc. Most of the scripts for `WIEN2k` are editable, and I have exploited this flexibility to make the calculations more accurate by, for example, adding spin-orbit coupling to some procedures that originally did not account for it.

# 2 Density Functional Theory and WIEN2k

In a many-electron system, the Hamiltonian in general consists of kinetic energy terms for electrons and ions, and potential energy terms for electron-electron, electron-ion and ion-ion interactions. Due to the inconveniently large number of terms, solving the Schrödinger equation fully is practically unachievable. The simplest approximation would be to assume that electrons do not interact with each other and to construct an effective potential by adding the screening effects of all other electrons to the ion potential, but this model is too primitive for our purpose. There are many other approximation strategies, but increased accuracy comes at a cost of computational time and memory storage. Among these approximations, the Hartree-Fock method [4] and the Density Function Theory [5, 6] are two of the most cost-effective approaches [7].

After the pioneering papers by Hohenberg, Kohn and Sham in 1964 and 1965 [5, 6], many approaches have been developed to implement DFT on a computer. With the need for efficient numerical calculations, much development has occurred in the field in the past 50 years, including the Augmented Plane Wave (APW) method [8], and the Linearised Augmented Plane Wave (LAPW) method [9] which combines the advantages of APW and the Orthogonalised Plane Waves (OPW) methods.

The `WIEN2k` package is a series of Fortran programs designed to solve the Kohn-Sham equations in DFT (see Appendix A). It uses full-potential (linearised) augmented plane wave and local orbitals basis set [10–12]. Within this package, there are several choices for the exchange-correlation energy functional, $V_{xc}$, including Perdew-Burke-Ernzerhof Generalised Gradient Approximation (PBE-GGA), Local Spin Density Approximation (LSDA), and Wu-Cohen-Generalised Gradient Approximation (WC-GGA) [13]. Since none of these methods are exact, the solution depends on which approximation is used [14] and which works the best depends on the specific system.

In this project, all calculations were carried out using PBE-GGA, and the precision was checked by increasing the number of wavefunctions in the basis set as well as the number of k-points until the results converged to the desired number of significant figures.

`WIEN2k` employs Self Consistency Field (SCF) cycles [15]. In order to solve the eigenvalue equation $\hat{H}\phi(\boldsymbol{r}) = E\phi(\boldsymbol{r})$, the potential function $V(\boldsymbol{r})$ (which is part of $\hat{H}$) is required; to obtain $V(\boldsymbol{r})$, however, the distribution of electrons, $\rho(\boldsymbol{r})$, is needed; to get $\rho(\mathbf{r})$ though, we need $|\phi|^2$, which can only be obtained by solving the eigenvalue equation. Therefore, to solve the equation, iterative steps must be used. Appendix B shows a summary of data flow during a SCF cycle. Each SCF cycle increases precision, and there are a few number of ways of choosing the terminating criterium including, for example, energy convergence and charge convergence. In this project, the terminating criterium was chosen to be energy convergence to within 0.00001 Ry.

In `WIEN2k`, *RKmax* stands for 'the product of the smallest atomic sphere radius, or Radius of Muffin Tin (RMT), and the largest **k**-vector (of the plane wave expansion of the wave function)' [16]. A larger RKmax value gives more accurate results, but there is a limit to how large it can be. The basis set scales with RKmax cubed, so a slight increase of RKmax will increase the time and memory cost of the computation tremendously. Therefore, multiple factors need to be considered before choosing it, including, for instance, the computing power and the size of the atomic spheres [16]. All RMT's were chosen to be same throughout this project since differing RMT might lead to different offsets (which are arbitrary) to the results [2].

For some packages in `WIEN2k`, the choice of implementing spin-orbit coupling was provided. For the ones which did not provide the function, scripts were edited to account for the coupling effect.

# 3 Bi-I

With atomic number 83 and electron configuration [Xe] $4f^{14}$ $5d^{10}$ $6s^2$ $6p^3$, bismuth in its phase I is a pentavalent semimetal. The electrical resistivity of Bi-I under pressure has been investigated by many research groups (see, e.g. [17]). At the QM group, however, the measurement was done at significantly more pressure values and at temperatures from 2K to 300K [3]. Since `WIEN2k` does not incorporate thermal effects, the values at 2K would be the most relevant.

## 3.1 Structure

Bi-I has a rhombohedral unit cell with experimentally measured parameters a = b = 4.546Å, c = 11.862Å, $\alpha = \beta = 90°$, and $\gamma = 120°$ at ambient pressure and room temperature [18]. Figure 2 shows two side-views of the structure. It has space group number 164, or $P\bar{3}m1$ in the Hermann-Mauguin notation [19].

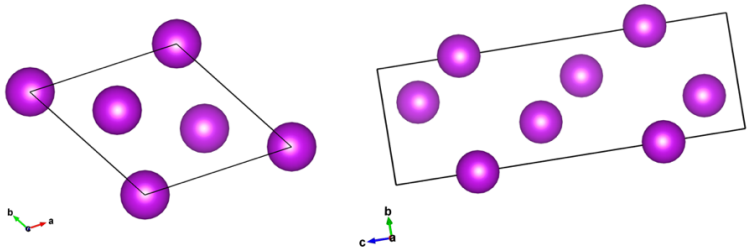

*Figure 2: View of Bi-I structure along c-axis (left) and a-axis (right).*

## 3.2 Pressure Simulation

To simulate variation of properties with pressure on a computer, it is sufficient to vary the lattice constants. To determine what the lattice constants should be for given pressures, we require

$$p = B\frac{V}{V_0},$$

where p is pressure, B is bulk modulus, V is the volume of a sample and $V_0$ is the volume of the sample at zero pressure. However, in computer modelling, an infinite-extent periodic structure is used; therefore, V and $V_0$ are for a unit cell instead.

Now, to obtain the relationship between p and V, the values of B and $V_0$ need to be calculated first. This is done by computing the energy stored per unit cell for different cell sizes. Integrating

$$dE = -pdV,$$

taking E = 0 at zero pressure, and substituting the previous equation, we arrive at

$$E = \frac{B}{2V_0}(\Delta V)^2,$$

where $\Delta V = V - V_0$. Alternatively, expanding $\Delta V$ gives

$$E = \left(\frac{B}{2V_0}\right)V^2 + bV + c,$$

b and c being the coefficients. Therefore, from a plot of E against V, we can easily obtain $V_0$, which is the value of V at the minimum, and the value of B follows.

Figure 3 shows the plot used to obtain the necessary numbers for Bi-I. Using `MATLAB`, a quadratic fit was applied to the data. From the coefficients, $V_0$ equals 1468.8 $(a.u.)^3$ and the bulk modulus was found to be 41.5 GPa. Compared with the measured range of 31 to 36 GPa by *AZo Materials* [20], and given that the range was not intended to be valid for extreme conditions such as zero temperature and extremely high pressures, the value of the obtained bulk modulus can be considered reasonable.

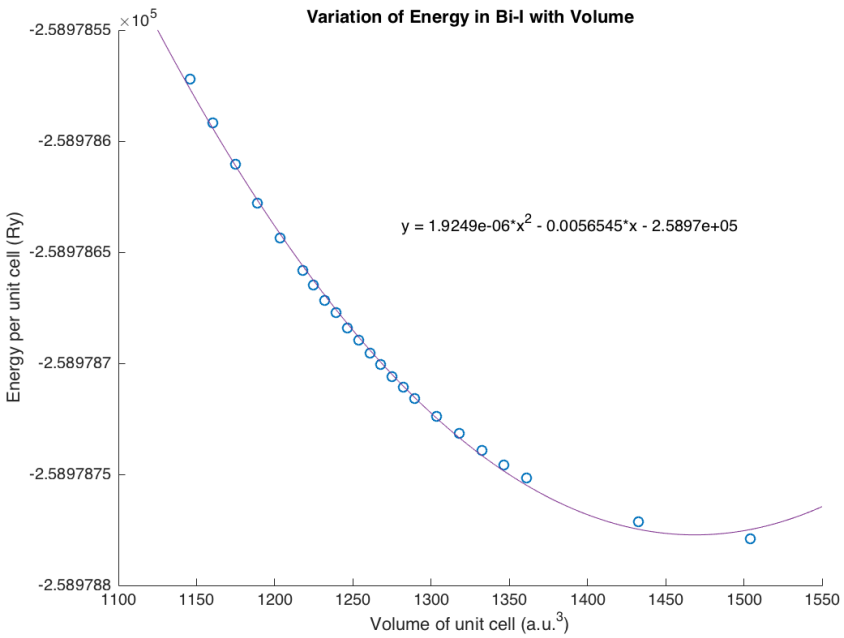


*Figure 3: Variation of energy per unit cell in Bi-I with volume of the unit cell and its second-order polynomial fit.*

## 3.3 Carrier Density at Ambient Pressure

At temperature of 2 K and ambient pressure, the carrier density of Bi-I was estimated from experimental measurements (e.g. of the Hall effect) to be of the order of about 1 carrier in 100,000 atoms. To explain this, the Fermi surfaces of Bi-I were obtained (see Figure 4). Spin-orbit coupling was included, as described in Section 2.

As can be seen from the diagram, there are two pockets at the centre of opposite hexagonal faces. These are hole pockets. It was checked by comparing the energy of the k states inside the pocket with Fermi energy. Similarly, on each of the edges, there is an electron pocket. Due to charge neutrality of the material, the volume of three electron pockets added together should equal the volume of one hole pocket.

Here the conventional reciprocal space unit cell is used, but, if desired, the primitive one can also be used. Fortunately they have the same volume (See Figure 5), so there is no need to know which convention was adopted by `WIEN2k` as far as volume is considered.

To calculate the carrier density at zero temperature, only the two bands crossing the Fermi energy level contribute. Given the Fermi surfaces, for each band, the number of charge carriers per bismuth atom can be calculated by

$$\frac{\dfrac{\text{occupied/unoccupied volume in each reciprocal unit cell}}{\text{total volume of the reciprocal unit cell}} \times 2}{\text{number of atoms in each real space unit cell}},$$

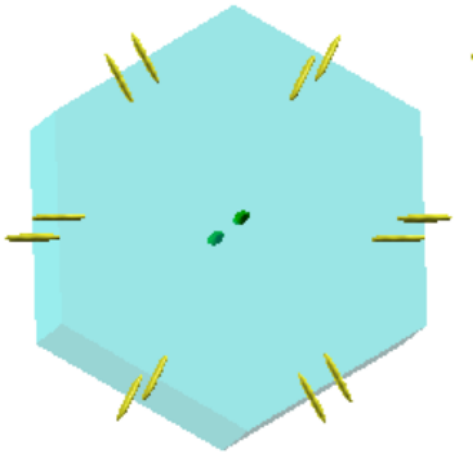

*Figure 4: The Fermi surfaces of two half occupied bands. The green ones are unoccupied, so there is a hole pocket per Brillouin zone, while the yellow ones are filled states, so there are 3 electron pockets per Brillouin zone.*

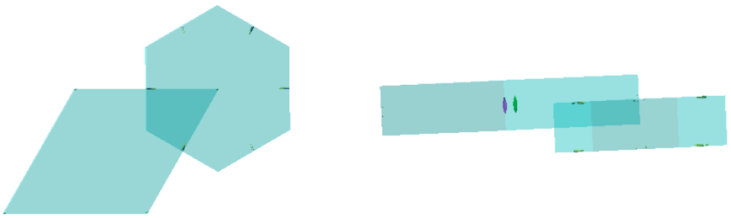

*Figure 5: Two choices of reciprocal space unit cells. The subfigure to the left has the c-axis perpendicular to the plane of the paper, while the one to the right has the c-axis pointing up in the plane of the paper. The rhombohedral unit zone corresponds to the primitive real space unit cell which is also rhombohedral, while the hexagonal zone corresponds to the conventional real space unit cell which is also hexagonal. Notice that the two zones have the same volume.*

where for the hole band we take the unoccupied volume and vice versa. The factor of two comes from the fact that each full band contributes to two electrons per real space unit cell due to electron's spin of 1/2 and the Pauli Principle. `SKEAF` was used to numerically compute the volumes of the carrier pockets in k-space.

At ambient pressure, the carrier density was computed to be about one carrier per 6,000 atoms, compared to about one in 100,000 atoms obtained experimentally. The large discrepancy is most likely due to the magnitude of the numbers. Since the carrier density is extraordinarily small, a very small error can lead to a large percentage error.

### 3.4 Semimetal to Semiconductor Transition

At the QM group, the resistivity of Bi-I was measured at temperatures from 2 K to 300 K under pressures up to 2.5 GPa. Figure 6 shows the results of the measurements. For high pressures, the variation of resistivity with temperature behaves like that of a semiconductor, while for low pressures it behaves like that of a metal. This indicates a metal/semimetal to semiconductor transition.

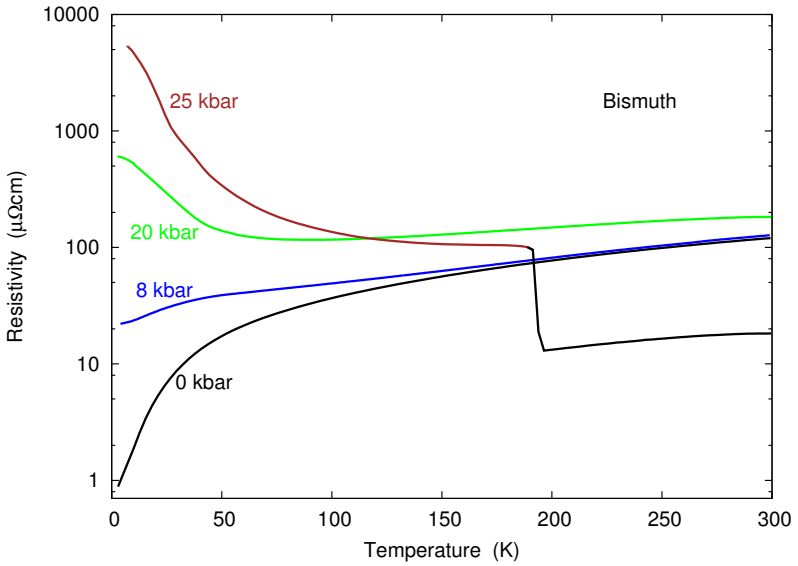


*Figure 6: Variation of resistivity with temperature at multiple pressures. The step for the curve at 25 kbar is due to the transition to Bi-II. The pressure dependence of the curves show a shift from metallic/semimetallic behaviour to semiconducting behaviour.*

Computationally, the carrier density in Bi-I was found to decrease with pressure. Figure 7 shows the computed carrier density of Bi-I at different pressures. The overall trend successfully explains the existence of the transition. However, the figure shows that the transition to the semiconducting behaviour happens at $(4.6 \pm 0.4)$ GPa, while the experimental results indicate a transition at $(1.4 \pm 0.6)$ GPa. Anomalies at about 1.0 and 4.2 GPa are not experimentally detected. The reason for this is unknown (see Section 8).

# 4 Bi-III

Between 2.8 and 7.7 GPa, bismuth is reported to have a stable phase, namely Bi-III [21]. Due to the complexity of its X-ray diffraction pattern, no *simple* model was able to fully account for all the features in the pattern. In 1972, Duggin *et al.* reported its structure to be tetragonal [22], but it could not fully explain the diffraction pattern. Similarly,

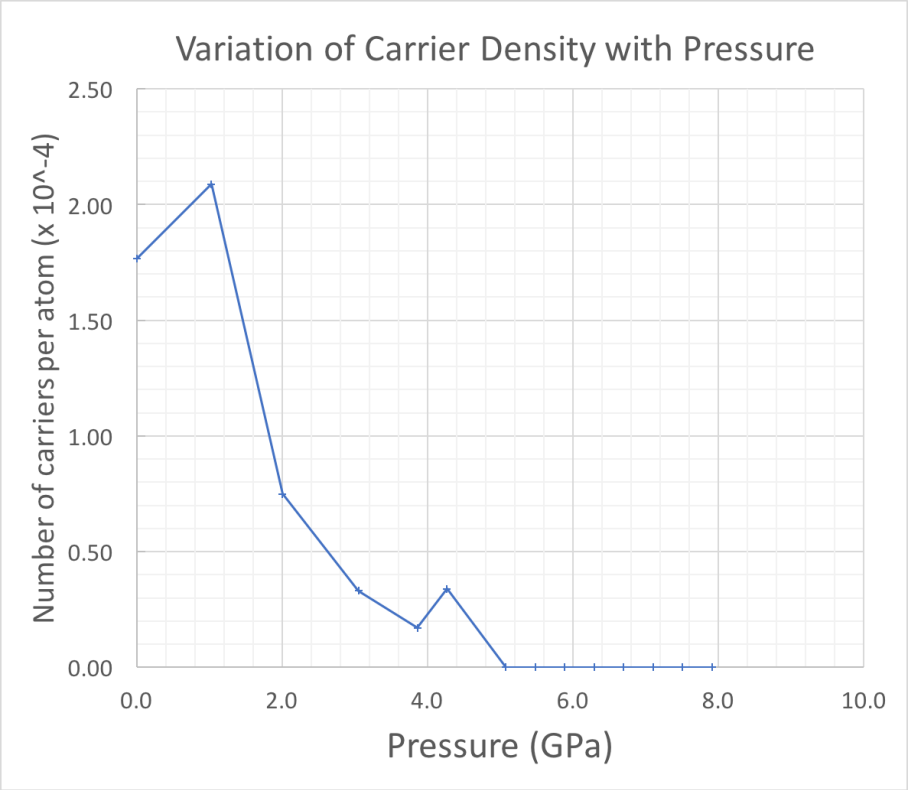


*Figure 7: Computed variation of carrier density of Bi-I per atom with pressure. There are two unexplained deviations from the overall decreasing trend at about 1.0 and 4.2 GPa. The carrier density reached and remained at 0 after about 5.0 GPa up to about 8.0 GPa, which indicates a band gap.*

in 1996, another attempt by Chen *et al.* also assumed that Bi-III took a tetragonal form, accounting for all but two of the major peaks in the pattern [23]. In addition, the model requires an unexplained volume *increase* for transition from Bi-II to Bi-III [21]. In 2000, McMahon *et al.* proposed an 'incommensurate host-guest model' which was more complicated but fitted the diffraction pattern very well[21].

Just before 2000, the incommensurate host-guest model was found for the first time in barium [24] and strontium [25], but was never found in a group V metal before. Computationally, I further investigated this model.

## 4.1 Description of the Model

The model consists of two categories of bismuth atoms - 'host' and 'guest'. The host component has a body-centred-tetragonal (bct) unit cell and so does the guest. What is special about this model is that the guest is incommensurate with the host along the tetragonal c axis, or the z direction, i.e. the ratio of the c parameters is not rational. The immediate result is the absence of a finite-sized unit cell. I created approximate structures

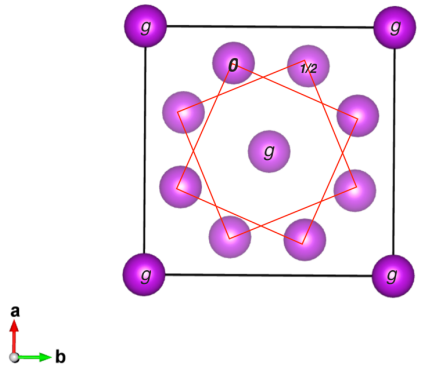


*Figure 8: A view along the c axis visualised using* **VESTA**. *The host atoms are placed at the corner of the two red squares which are at $z = 0$ and $z = 1/2$ respectively. Repeating the cells in z-direction creates tunnels in which the guest atoms (labelled 'g') reside.*

that do have unit cells, expecting that the properties of the actual model can be predicted with increasing accuracy as the approximation improves.

## 4.2 Approximate Models

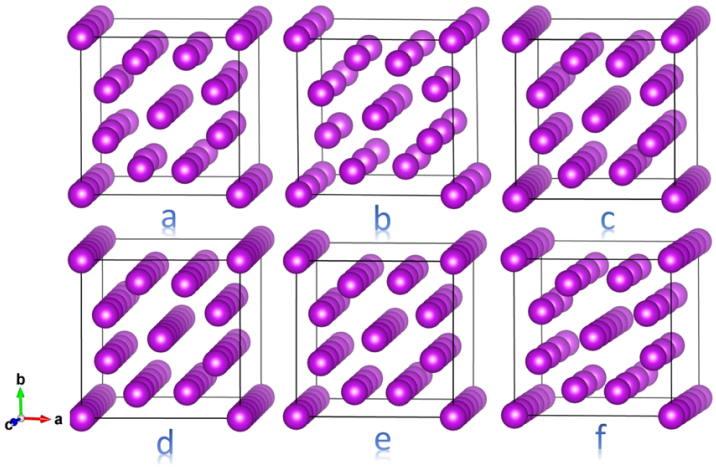


*Figure 9: A view of six approximate models from a direction almost parallel to c axis. Note the ratio of numbers of guest atoms and host atoms along c axis.*

The six approximate models created are shown in Figure 9. An important factor in determining how closely each of them resembles the incommensurate model is the ratio of the c parameters for the guests and the hosts, $c_H/c_G$. Limiting the number of atoms in a unit cell to less than 60, these are all the six possible approximate models that can be created while having a reasonable $c_H/c_G$. Figure 10 compares the ratios for each of the models and how close they are to the measured ratio which is 1.309 [21]. The number

of atoms in the unit cell is also shown next to the bar chart for each of them. The best approximate model, Bi-IIIa, which has a less than 2% difference from the measured $c_H/c_G$ ratio, has only 32 atoms per unit cell. This is a fortunate coincidence. (Ba-IV, for example, has a measured $c_H/c_G$ ratio of 1.378, and at least 54 atoms per unit cell are required to achieve a difference of less than 2%.) In practice, 32 atoms per unit cell is a reasonable number since most computations on this model can be done within a day with the available computer.

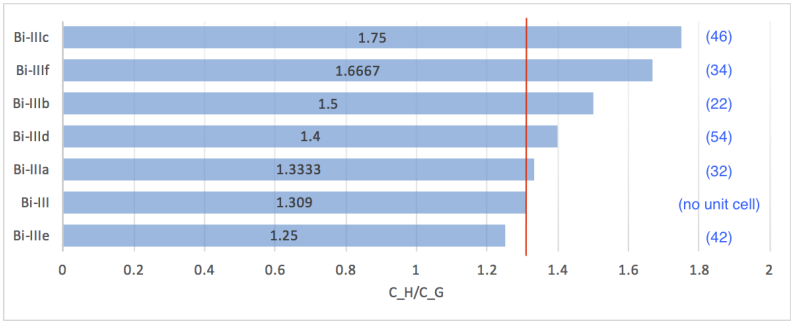


*Figure 10: A bar graph comparing $c_H/c_G$ values of the approximate models. Bi-III is the model with measured incommensurate ratio of 1.309. The numbers in brackets show the number of atoms in each unit cell.*

With the computer at the QM group (Intel Core i5-2500 CPU @ 4x 3.301GHz), energy convergence criterium chosen as 0.00001Ry, 1000 points in k-mesh, and RK-max equalling to 7, for a unit cell with 54 atoms, self consistency field (SCF) iterations take about 24 to 36 hours to complete. Running volume optimisation to model pressure change requires carrying out the same tasks N times with different lattice parameters where N is the number of pressure points needed (usually N = 5). Therefore, each round of pressure simulation can take up to half a week to run and consequently models with larger unit cells were not simulated in this project.

## 4.3 Metallic Property

The measured electrical conductance of Bi-I just above the Bi-II-III transition pressure was about twice of that of Bi-I just below the Bi-I-II transition pressure [17]. This metallicity can be theoretically confirmed by looking at the density of states. The density of states can be simply calculated from the bands obtained from `WIEN2k` by adding up the contribution from each band at each energy level. Using 5000 k-points, RK-max being 7, PBE-GGA method, energy convergence to within 0.00001 Ry, and including spin-orbit coupling, Figure 11a was obtained. It shows the density of states plot for Bi-IIIa, the most accurate model among the six. Similarly, the density of states plot for Bi-IIIe, the second most accurate model, was calculated and displayed in Figure 11b.

Despite the differences, both plots show strong metallicity. For both models, the Fermi level lies at a non-negligible energy above the gap. Since the measured $c_H/c_G$ ratio lies in

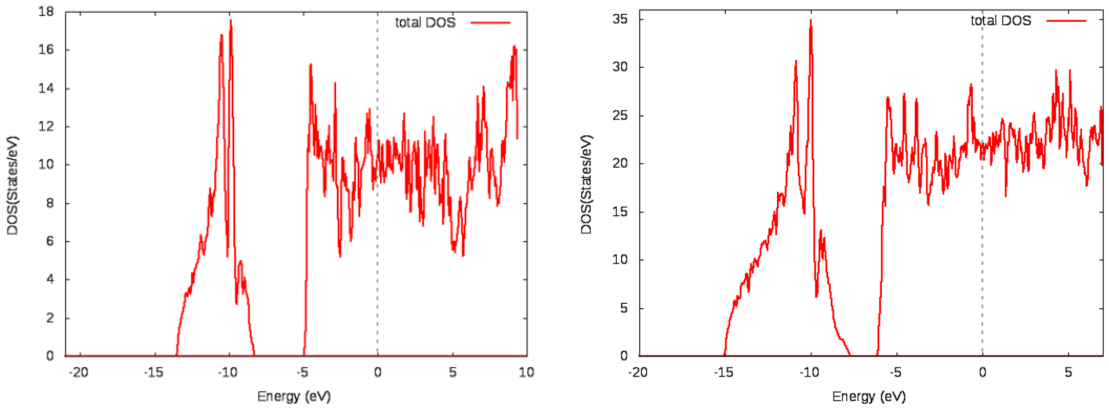


*(a) Bi-IIIa* *(b) Bi-IIIe*

*Figure 11: Density of states (per unit cell) plots for two approximate models of Bi-III. Fermi energy has been calibrated to be zero. Note that the values at Fermi level are non-zero.*

between these two, it is reasonable to deduce that Bi-III should be a metal with a similar density of states plot.

### 4.4 Plasma Frequency

The plasma frequency of a material is informative in that it can be used to compute the lifetime (in the context of collisions) of the carriers given the conductivity of the material since

$$\Omega_p^2 = \frac{ne^2}{m^*} \text{ and } \sigma = \frac{ne^2\tau}{m^*},$$

where $\Omega_p$ is the plasma frequency, $n$ is the carrier density, $m^*$ is the effective mass of the carrier, and $\tau$ is the lifetime of the carrier.

The plasma frequency for a model can be obtained using the OPTIC package from `WIEN2k` once SCF cycles are done. Figure 12 shows the computed plasma frequencies for a few models with different $c_H/c_G$ ratios. With this, the plasma frequencies for Bi-III are estimated to be $(3.8 \pm 0.1)$ eV along a direction perpendicular to the symmetry axis and $(4.5 \pm 0.5)$ eV along the symmetry direction.

## 5 Bi-I v.s. Bi-III

Comparing the energies stored per unit cell helps understand why the phase transition from Bi-I to Bi-III occurs. In this project, Bi-II is not investigated, but since it only

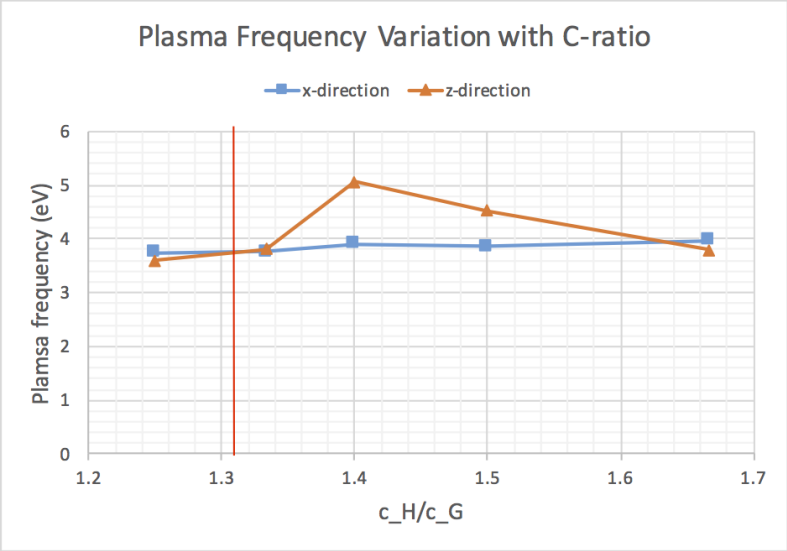


*Figure 12: Plasma frequency plotted against $c_H/c_G$ ratio for both x-direction and z-direction. The red line indicated the position of measured ratio.*

occupies a very short range along the pressure axis, it does not affect a comparison between Bi-I and Bi-III.

After obtaining the relationship between volume and pressure (using the method described in Section 3.2), the previous energy-volume curves can be translated to energy-pressure curves (while carefully taking into account of the difference in the number of atoms per unit cell). Plotting these curves for Bi-I and three approximate structures on the same graph gives Figure 13.

From the graph, the Bi-I curve crosses Bi-IIIe, Bi-IIIa and Bi-IIIb curves at pressures 8.0, 8.8 and 10.0 GPa respectively. This order, interestingly, is also the order of increasing $c_H/c_G$, suggesting a positive correlation between $c_H/c_G$ and the pressure at curve crossing. Since the experimentally measured value of $c_H/c_G$ lies between that of Bi-IIIe and Bi-IIIa, interpolation gives an intersection of Bi-I and real Bi-III at a pressure between 8.0 and 8.8 GPa.

At the low pressure extreme, the Bi-III structure is not favoured energetically. Above the crossing point, however, Bi-III is lower in energy per atom than Bi-I. So this qualitatively explains why the phase transition occurs. Quantitatively, the value does not agree with the experimentally observed fact that the transition occurs at about 2.5 GPa. This discrepancy might be ascribed to the following reasons:

a. Interpolation does not apply here. The fact that the three approximate models crossed the Bi-I curve in an order related to that of $c_H/c_G$ is coincidental. (While this may be true, it seems very unlikely that the actual crossing point will be at a pressure much lower than 8 GPa.)

b. The transition is not driven by energy.

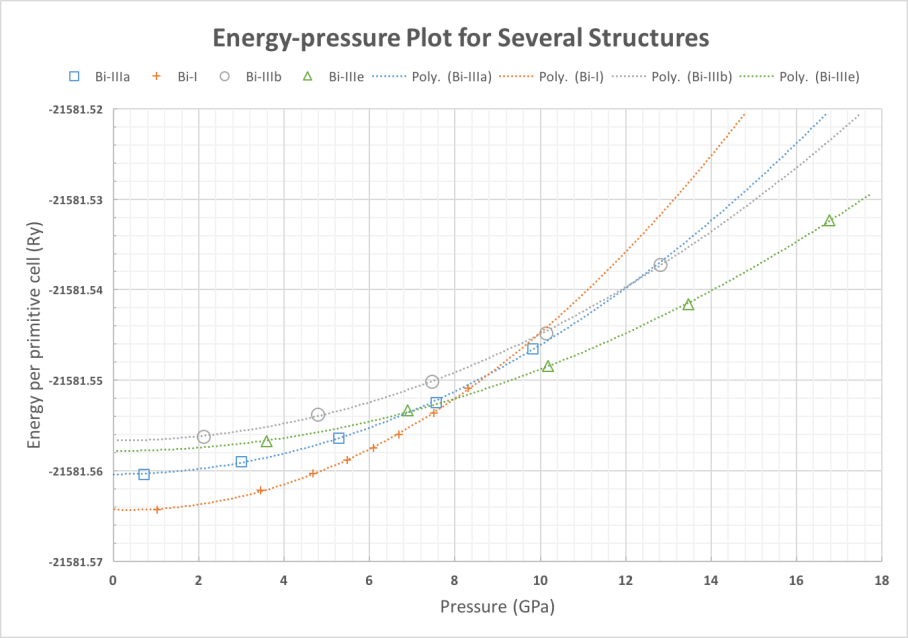


*Figure 13: A plot of simulated energy versus pressure for Bi-I and three models of Bi-III. A quadratic-fit curve is displayed for each of them. The Bi-I curve crosses the other three at about 8 to 10 GPa. Below the crossing, Bi-I is lower in energy, while above it, the Bi-III structure is lower in energy.*

c. The incommensurate model assumes chains of guest atoms being able to slide in channels of host atoms, but all the models used above do not allow the relative positions to change. It is possible that the mobility of chains plays a major role here.

# 6 Comparison with Ba-IV

As mentioned in Section 4, the host-guest incommensurate structure was also found in barium in its phase IV [24]. However, the atomic sizes, number of (outer-shell) electrons, lattice constants, and, most importantly, $c_H/c_G$ ratios are different for the two materials; therefore, it is worth investigating whether the host-guest incommensurate structure can be divided into finer sub-categories, or, in addition to that, what properties of the material result in such a peculiar structure.

As an attempt to achieve that, the Fermi surfaces of the two structures can be compared. The plan was to see, firstly, whether the Fermi surfaces of Bi-III and Ba-IV are similar. If they are, then it hints at a possibility that all host-guest incommensurate structures arise due to a particular shape of the Fermi surface, or, equally, the configuration renders Fermi surfaces of particular shapes regardless of the atom. Secondly, it is worth finding out whether the Fermi surfaces are close to the Brillouin zone boundary. If so, it can help

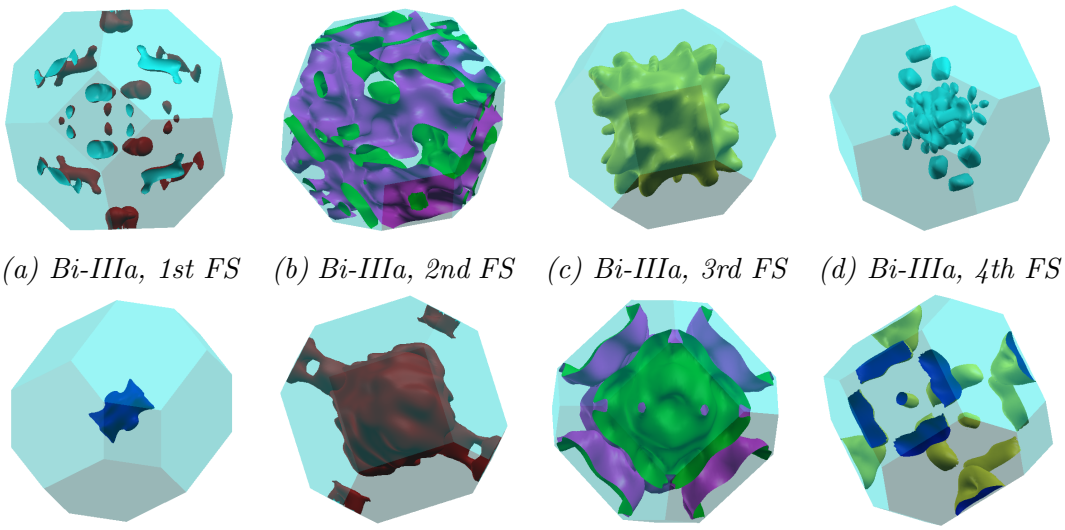

*(a) Bi-IIIa, 1st FS* *(b) Bi-IIIa, 2nd FS* *(c) Bi-IIIa, 3rd FS* *(d) Bi-IIIa, 4th FS*

*(e) Ba-IVa, 1st FS* *(f) Ba-IVa, 2nd FS* *(g) Ba-IVa, 3rd FS* *(h) Ba-IVa, 4th FS*

*Figure 14: Fermi surfaces of Bi-IIIa and Ba-IVa shown in the first Brillouin zone, represented in the colour cyan. In each subfigure, the same side of each Fermi surface is represented by the same colour.*

explain the formation of the host-guest structure (a generalisation of the one-dimensional Peierls Theorem [2]). For example, hydrogen-like atomic chains, by distorting the inter-atomic distances, can lower the overall energy of the system. The same principle might apply here. If the transformation to host-guest structure causes changes in the band structure such that two bands near Fermi energy shift, one up and one down, then the total energy of the system will decrease. In addition, the band structure, in particular the Fermi surfaces obtained, might be used by other researchers to explain other properties of Bi-III and Ba-IV.

At 12.9 GPa, Bi-IV has a $c_H/c_G$ ratio of 1.378, not very different from that of Bi-III at 6.8 GPa (1.309). This means that the model Bi-IIIa can be modified to approximate the structure for Ba-IV. Figure 14 shows the Fermi surfaces obtained for models Bi-IIIa and Bi-IVa (same as Bi-IIIa but with Bi atoms replaced by Ba atoms and adjusted lattice parameters).

A glance at Figure 14 shows that there are four bands crossing the Fermi energy for both materials, which is one similarity between the two materials. Nevertheless, the Fermi surfaces for structural models Bi-IIIa and Ba-IV are clearly very different. This shows that host-guest incommensurate structures do not necessarily have the same or similar Fermi surfaces. However, care must be taken at this point since the models are only approximate.

Looking at the Fermi surfaces closely, panels (b) and (g) show Fermi sheets close to the Brillouin zone boundary, but it is not the case for the other bands. Therefore, it is not clear whether the energy-lowering mechanism described earlier can be exploited for

explanation of the formation of host-guest incommensurate structure.

# 7 Conclusion

In conclusion, several properties of Bi-I and Bi-III were calculated using DFT, including the carrier density at ambient pressure for Bi-I, semimetal to semiconductor transition of Bi-I, metallicity of Bi-III, plasma frequency for Bi-III and relative energies for Bi-I and Bi-III under different pressures. A comparison of the Fermi surfaces of Bi-III and Ba-IV was also attempted.

Computations explained that the electrical resistivity increases with pressure, that Bi-I changes into a semiconductor at a certain pressure, and that Bi-III is a metal. However, quantitative data did not compare well with the experimental results, including the pressure at which Bi-I changes from semimetal to semiconductor, the pressure for Bi-I to Bi-III transition, and the carrier density at ambient pressure. No firm conclusion can be drawn from the Fermi surfaces obtained for Bi-III and Ba-IV.

The main features of this project include simulating pressure variation and modelling the incommensurate structure with approximate models. The quantitative discrepancies might be attributed to inadequacy of the models, invalidity of assumptions of DFT, etc.

# 8 Further Investigation

The limited time of the project did not allow a thorough study of the points touched on in this report. There are a few important things that could be done to further investigate them. The following list gives a few:

a. Computation with `WIEN2k` gives very high precision, but its accuracy is not quantified. To make a quantitative error analysis, one could try different exchange correlation functions or alternative approaches to DFT to see how close their results can be.

b. Since most of the quantitative results did not agree with the experiment, there must be a large room for improvement of the model. DFT and `WIEN2k` works well for many material structures, but they might need to be improved for particular cases, such as when the carrier density is extremely small or when no unit cell exists.

c. The anomalies on the carrier density variation with pressure requires further computation. If the random errors can be quantised, then we can tell whether the anomalies are due to random errors. If they are not due to random errors, then systematic errors should be checked, including the validity of DFT for this case.

d. To further investigate similarities of Bi-III and Ba-IV, much larger unit cells can be used which will take significantly more computing time and memory. By approaching the correct $c_H/c_G$ with even larger unit cells, one might be able to either confirm that their Fermi surfaces diverge or that they start to resemble each other when the ratio is accurate enough. In either case, it is important to find out whether there is a simple link between the formation of host-guest incommensurate structure and the band structure of the material.

# 9 Acknowledgement

The author would like to thank Dr Malte Grosche for his mentoring and provision of this research opportunity. He is also thankful to Alex Vasiljkovic and Phil Brown for their kind help during the project.

# References


[1] F. M. Grosche. Quantum matter group website. `http://www.qm.phy.cam.ac.uk/`, 2014.

[2] F. M. Grosche. Personal Correspondence, September 2016.

[3] A. Vasiljkovic. Personal Correspondence, September 2016.

[4] D. R. Hartree. The calcualtion of atomic structures. *Acta Crystallographica*, 11:376, 1958.

[5] P. Hohenberg and W. Kohn. Inhomogeneous electron gas. *Physical Review*, 136, June 1964.

[6] W. Kohn and L. J. Sham. Self-consistent equations including exchange and correlation effects. *Physical Review*, 140:A1133, November 1965.

[7] K. N. Kudin and G. E. Scuseria. Converging self-consistent field equations in quantum chemistry - recent achivements and remaining challenges. *ESAIM: M2AN*, 41(2):281, 2007.

[8] J. C. Slater. Wave functions in a periodic potential. *Physical Review*, 51:846, May 1937.

[9] O. K. Andersen. Linear methods in band theory. *Physical Review B*, 12:3060, October 1975.

[10] P. Blaha, K. Schwarz, and P. Sorantin. Full-potential, linearised augmented plane wave programs for crystalline systems. *Computer Physics Communications*, 59(2): 399, 1990.

[11] K. Schwarz and P. Blaha. Solid state calcualtions using wien2k. *Computational Materials Science*, 28(2):259, October 2003.

[12] K. Schwarz, P. Blaha, and S. B. Trickey. Electronic structure of solids with wien2k. *Molecular Physics*, 108(21-23):3147, 2010.

[13] P. Blaha, K. Schwarz, G. Madsen, D. Kvasnicka, and J. Luitz. *User's Guide, WIEN2k 12.1*, 12.1 edition, July 2012.

[14] S. Cottenier. *Density Functional Theory and the Family of (L)APW-methods: a step-by-step introduction*, 2 edition, 2002-2013.

[15] P. Blaha. Recorded WIEN2k workshop at McMasters University. `http://www.wien2k.at/onlineworkshop/`, 2016.

[16] P. Blaha, K. Schwarz, and J. Luitz. Wien2k-faq: How to set a good rkmax value? `http://www.wien2k.at/reg_user/faq/rkmax.html`, 2001.

[17] J. R. Vaisnys and R. S. Kirk. Effect of pressure on the electrical properties of bismuth. *Journal of Applied Physics*, 38(11):4335, October 1967.

[18] C. S. Barrett. The structure of bismuth at low temperatures. *Australian Journal of Physics*, 13(2):209, June 1960.

[19] Th. Hahn. *International Tables for Crystallography Volume A: Space-Group Symmetry*. Wiley, 5 edition, 2005.

[20] AZo Materials, June 2001.

[21] M. I. McMahon, O. Degtyareva, and R. J. Nelmes. Ba-IV-type incommensurate crystal structure in Group-V metals. *Physical Review Letters*, 85(23), December 2000.

[22] M. J. Duggin. A high-pressure phase in arsenic and its relation to pressure-induced phase changes in Group 5B elements. *Journal of Physics and Chemistry of Solids*, 33(6):1267, 1972. doi: 10.1016/s0022-3697(72)80166-5.

[23] J. H. Chen, H. Iwasaki, and T. Ktkegawa. Crystal structure of the high pressure phases of bismuth Bi-III and Bi-III' by high energy synchrotron x-ray diffraction. *High Pressure Research*, 15(3):143, 1996. doi: 10.1080/08957959608240468.

[24] R. J. Nelmes, D. R. Allan, M. I. McMahon, and S. A. Belmonte. Self-hosting incommensurate structure of barium IV. *Physical Review Letters*, 83(20):4081, November 1999.

[25] M.I. McMahon, T. Bovornratanaraks, D. R. Allan, S. A. Belmonte, and R. J. Nelmes. Observation of the incommensurate barium-IV structure in strontium phase V. *Physical Review B*, 61(5):3135, February 2000.

# A Program Flow in WIEN2k

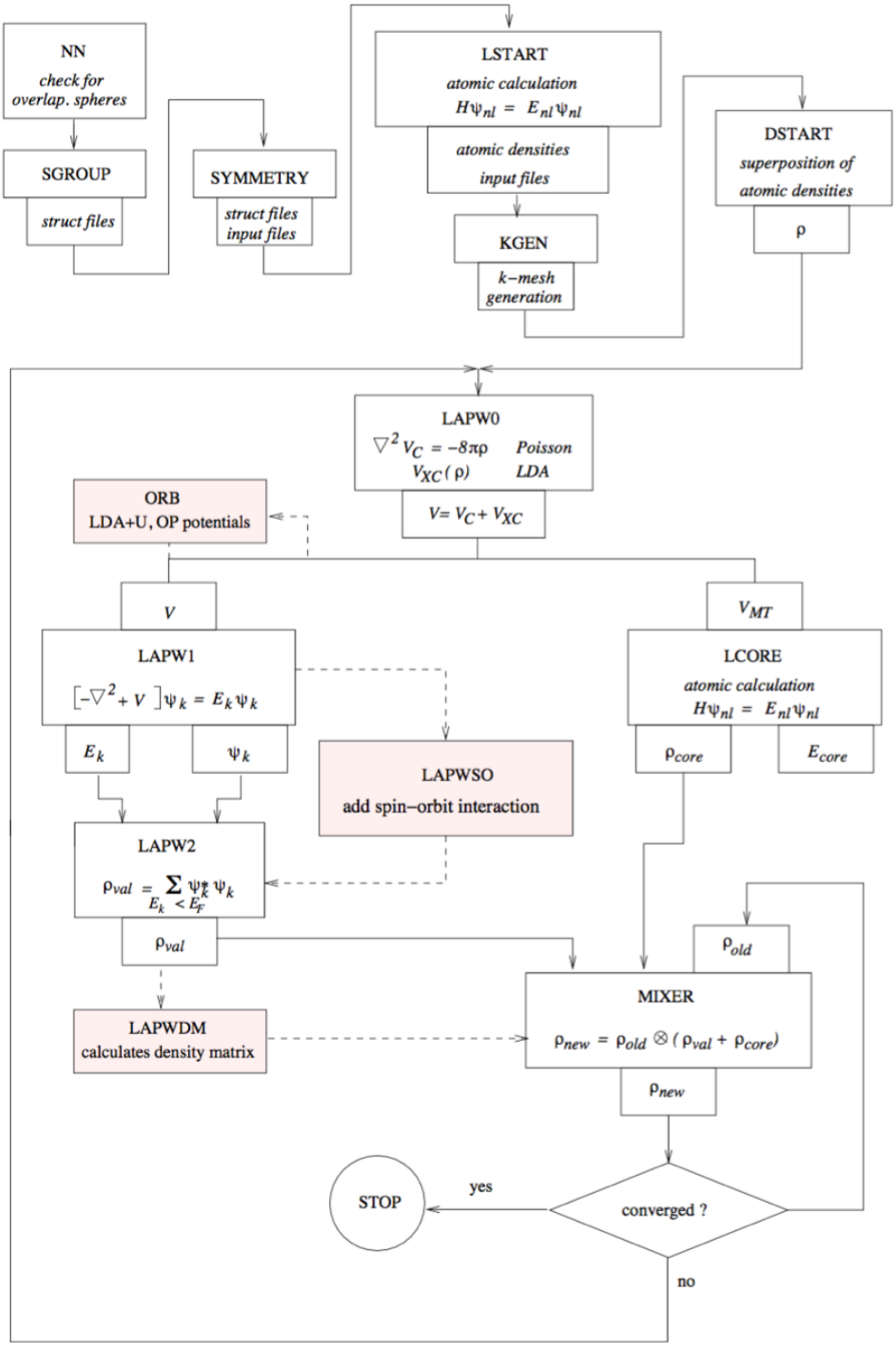


*Figure 15: Program flow in* **WIEN2k** *[13].*

# B Data Flow for a SCF Cycle

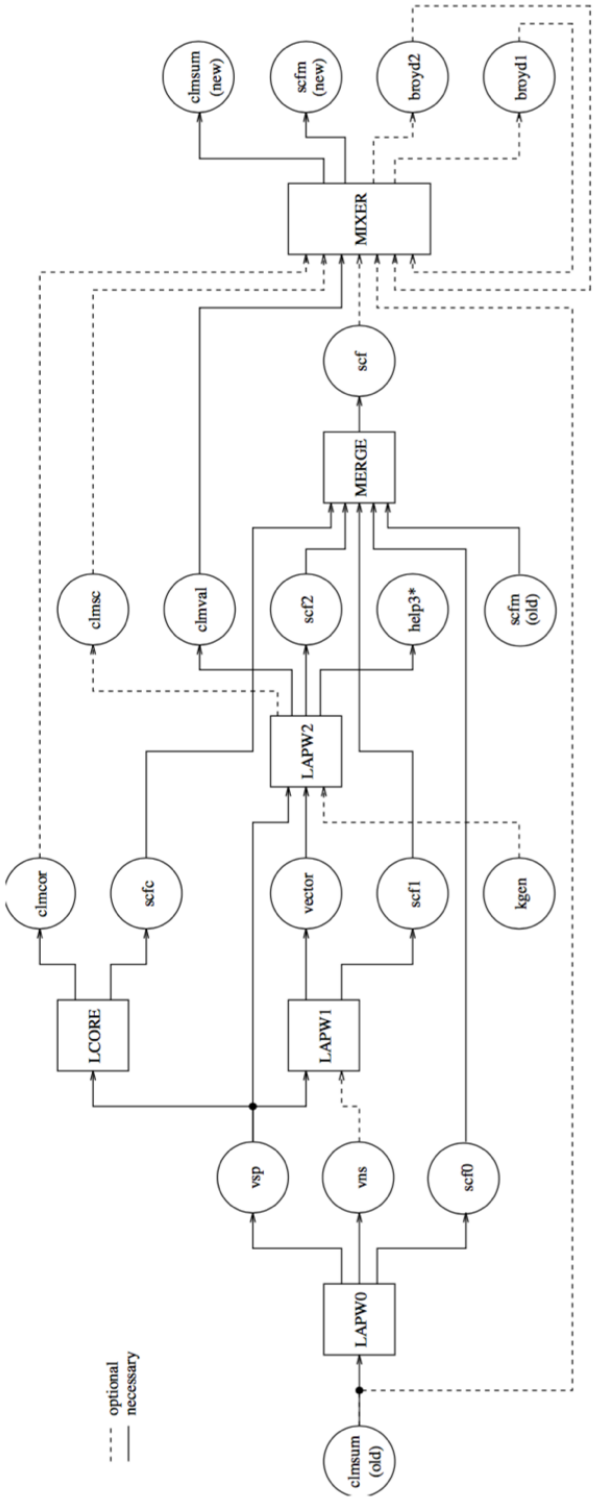


*Figure 16: Data flow during a SCF cycle (programX.def, case.struct, case.inX, case.outputX and optional files are omitted) [13].*